IEEE Access
Multidisciplinary | Rapid Review | Open Access Journal

Received April 29, 2021, accepted May 11, 2021, date of publication May 17, 2021, date of current version May 26, 2021.

Digital Object Identifier 10.1109/ACCESS.2021.3080823

A Dual-Band Circularly Polarized Elliptical Patch Reflectarray Antenna for High-Power Microwave Applications

GEXING KONG, XIANGQIANG LI, (Member, IEEE), QINGFENG WANG, AND JIANQIONG ZHANG

School of Physical Science and Technology, Southwest Jiaotong University, Chengdu 610031, China

Corresponding author: Xiangqiang Li (xiangqiang_li@swjtu.edu.cn)

This work was supported by the Fundamental Research Funds for the Central Universities under Grant 2682021CX072.

ABSTRACT The demand for multi-band high-power antennas, which have been rarely reported, becomes urgent in high-power microwave field. To meet the demand, a C/X dual-band high-power circularly polarized patch reflectarray antenna is proposed in this paper. Two main technologies are adopted to make the proposed antenna realize the high-power feature. Firstly, the elliptical patch with no abrupt structure is proposed to be the dual-band reflecting element to mitigate the electric field concentration. Secondly, the elliptical patches are proposed to be embedded into substrate to avoid the triple junction. The proposed dual-band reflecting element is designed by arranging two embedded elliptical patches with different sizes in a square lattice grid. The larger elliptical patch operates in C-band and the smaller one works in X-band. The elliptical patches are proposed to be rotated to realize continuous 360° phase response in both bands. By optimizing the thickness of substrate, the element spacing, and the size of the patches, the dual-band element shows good reflection amplitude and phase response and low mutual coupling performance. An antenna prototype with the aperture size of 345 mm × 345 mm is simulated and measured. The measured radiation results of the designed reflectarray antenna are in good agreement with simulations in both C-band and X-band. The measured gain of the antenna at 6.2 GHz is 24.6 dBi, and at 9.3 GHz is 27.8 dBi. Full-wave simulations show that the power capacity of the antenna at 6.2 GHz is about 10.2 MW, and at 9.3 GHz is about 3.9 MW in air condition. The low mutual coupling performance of the proposed antenna is verified both in element level and array level. All of the results show that the proposed antenna has the merits of high-power capacity, dual-band, and low mutual coupling.

INDEX TERMS Dual-band, embedded patch, high-power microwave, reflectarray antenna.

I. INTRODUCTION

With the development of high-power technology, the research on high-power array antennas promotes the applications for various military and civilian satellite communications [1]. The available high-power array antennas mainly focus on increasing the operating frequency [2], [3], improving the power capacity [4], [5], realizing beam scanning [6], and extending the bandwidth [7]. These technologies promote the development of high-power microwave antennas, but they can only operate in one frequency band. Based on the analysis of the existing literatures, there have been few reports on high-power antenna to cover two frequency bands. Dual-band reflectarray antenna is a good candidate to provide the coverage. In general, the dual-band reflectarray antennas can be divided into double-layer and single-layer configurations. The double-layer dual-band reflectarray antenna achieves the phase shift by adjusting the patches placed on the two substrate layers. However, the patches on the upper layer inevitably block the patches on the lower layer, which affects the performance of the antenna [8]. And the double-layer structure makes the weight and cost high. Single-layer dual-band reflectarray antenna has been widely studied for the advantages of low cost and eliminated shielding [9]–[13]. Typically, the representative single-layer dual-band reflectarray antennas include the dual split-loop antenna achieving

The associate editor coordinating the review of this manuscript and approving it for publication was Davide Ramaccia.

the phase adjustment in the two frequencies by rotating the inner and outer split rings [9], the square ring and slotted rectangular patch antenna realizing the phase adjustment by varying the size of element [10], the slotted circular patch with two phase delay line antenna changing the lengths of phase delay line to achieve the both bands' phase compensation [11]. These antennas realize the directional radiation in two frequency bands. But the patches with splits or slots are easy to cause the electric field concentration and restrict their power capacity. Up to now, the research on dual-band patch reflectarray antennas are mainly focused on the low-power microwave field, there have been few reports on high-power dual-band patch antenna.

Elliptical patch with no abrupt structure has the potential for high-power microwave applications. An elliptical patch reflectarray antenna has been proposed and the given electric field on the patch is much lower than that on the traditional patches with splits or slots [14]. In the design, the elliptical patch reflecting element achieves the phase adjustment by varying the dimension of the patch with S-shaped phase response curves. In this letter, a C/X dual-band high-power circularly polarized reflectarray antenna consisting of two kind of elliptical patches embedded into substrate is proposed. The elliptical patch element is proposed to be rotated to realize the linear phase response curves. The comparison with state-of-the-art single-layer dual-band reflecting elements verifies the performances of high-power and low mutual coupling. And the low coupling effect between the two band elements is further verified by comparing the radiation patterns of the single-band reflectarray antennas with that of the dual-band reflectarray antenna.

This paper is organized as follows. The design process of the proposed high-power dual-band element and the reflected amplitude and phase responses, and coupling effect of the element is analyzed in Section II. In Section III, the comprehensive simulated and measured results of a reflectarray antenna prototype are presented to verify the performances of dual-band, high-power capacity, and low mutual coupling. Finally, the conclusion is given in Section IV.

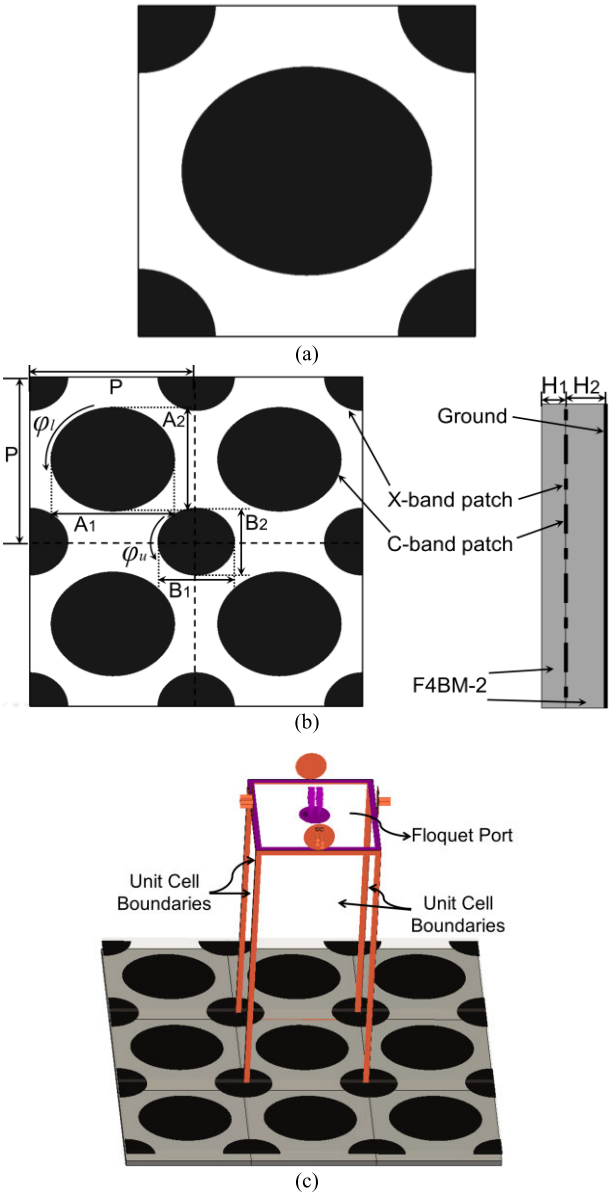

FIGURE 1. Configurations of (a) the proposed high-power dual-band embedded elliptical patch reflecting element, (b) periodic structure containing four dual-band elements, and (c) simulated model of the proposed element.

II. DESIGN OF THE DUAL-BAND REFLECTING ELEMENT

To design a dual-band reflecting element with low mutual coupling, and high-power capacity performances, there are three considerations as follows. First, the angular rotation technique is one of the popular methods to achieve the tunable phase shift, and this technique has a stable phase response inherently, which means that there is little mutual coupling on the reflected phase. Second, circular polarization is the basic of the angular rotation technique. The elliptical patch can radiate circular polarized wave and mitigate the electric field concentration for the patch having no abrupt structure. Third, comparing with the traditional reflecting elements with the patches exposed to the air, the patches embedded into substrate can avoid the triple junction and can improve the power capacity. Based on the above analysis, the high-power dual-band embedded elliptical patch reflecting element is proposed and deigned.

A. ELEMENT GEOMETRY

The configuration of the proposed high-power dual-band embedded elliptical reflecting element is shown in Fig. 1 (a) and the view of the periodic structure containing four elements is shown in Fig. 1 (b). The dual-band reflecting element is designed by arranging two embedded elliptical patches with different sizes in a square lattice grid. The patches are placed in the center or the corner of the element. The larger elliptical patch operates in C-band and the smaller one works in X-band. The distance between the adjacent patches with

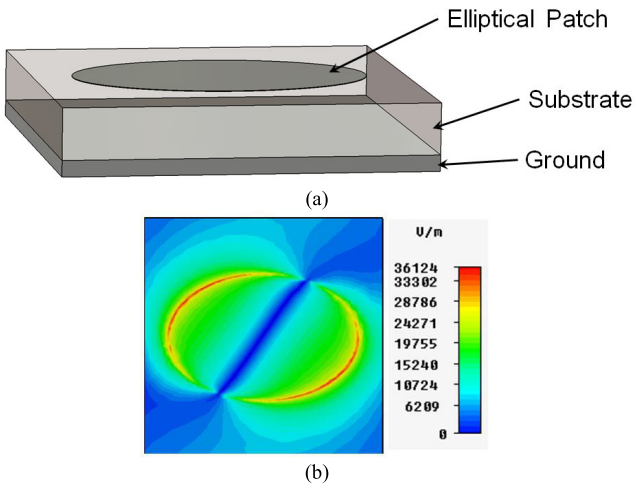

FIGURE 2. (a) Configuration and (b) electric field distribution diagram of the X-band traditional single elliptical patch reflecting element.

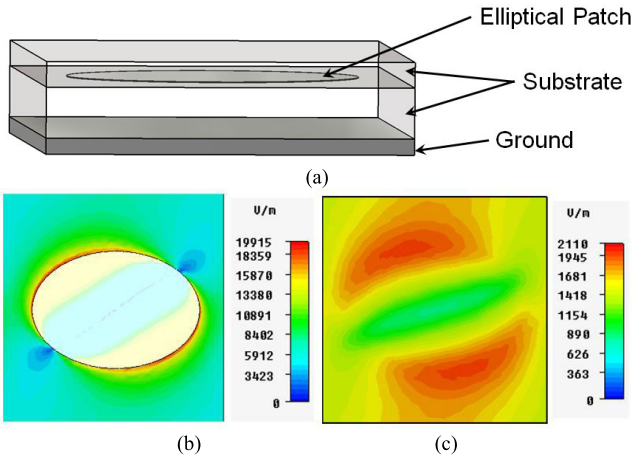

FIGURE 3. (a) Configuration and electric field distribution diagrams of (b) patch and (c) surface of the X-band embedded single elliptical patch reflecting element.

same dimension is equal to the element spacing. The patches are designed to be embedded into F4BM-2 substrate with dielectric constant of 2.2, loss tangent of 0.001.

First, an X-band traditional single elliptical patch reflecting element is designed as shown in Fig. 2 (a). The preliminary dimensions of the patch can be calculated by the formulas in [15]. And the element is simulated under the left-handed circularly polarized plane wave excitation. The obtained electric field distribution diagram of the element is shown in Fig. 2 (b). The maximum electric field is lower than that in [14], but is still higher than that of the high power element [7]. The design with no triple junction can improve the power capacity [16]. So the traditional single elliptical patch reflecting element is modified with the patch embedded into substrate. The configurations of the embedded single elliptical patch reflecting element and the obtained electric field distribution are shown in Fig. 3. It can be found that the maximum electric field strength of the embedded patch

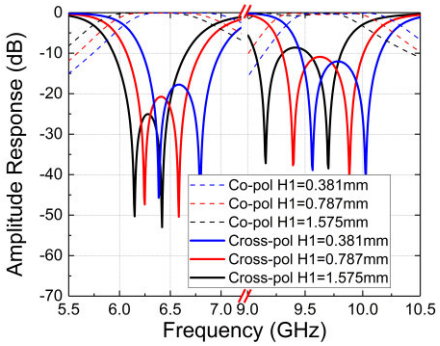

FIGURE 4. Reflected amplitude of the proposed dual-band embedded elliptical patch reflecting element for different thicknesses of upper substrate.

is about half of that of the traditional element, and the electric field on the surface is significantly reduced. The compared results prove that the proposed embedded elliptical patch reflecting element shows high power capacity feature. It should be pointed out that the electric field on the surface would further reduce with a thicker substrate, but the available bandwidth would be changed. The reflected amplitude of the dual-band reflecting element with different commercially available thicknesses of upper substrate H_1 are shown in Fig. 4, with the thickness of the lower substrate H_2 selected to be 1.575 mm. With H_1 increases, the available bandwidth of the two bands move toward the lower frequency and the cross-pol reflected amplitude of X-band become deteriorated. The relative good reflected amplitude for the two bands can be obtained with H_1 is 0.787 mm.

To confirm the circularly polarized wave radiation performance of the elliptical patch reflecting element, the X-band embedded single elliptical patch reflecting element as shown in Fig. 2 (b) is simulated under the horizontally and vertically polarized plane wave incidence. The obtained electric field distribution diagrams of the surface of the element are shown in Fig. 5. Two orthogonal TM_{01} modes are excited on the surface of the element. For elliptical patch, given that the effective length in the two orthogonal directions is different, the 90° phase difference between the two orthogonal TM_{01} modes can be achieved with an appropriate size and the circularly polarized wave can be reradiated. Therefore, the phase of the reflected wave can be adjusted by rotating the elliptical patch when the element is exited by the circularly polarized plane wave [17].

Generally, the suggested element spacing is half wavelength at high frequency in order to avoid grating lobes at both bands. Due to the two bands' elements are arranged in a square lattice grid, so a slightly larger element spacing is adopted, which contribute to the low coupling effect and also can reduce the electric field on the surface. The reflected amplitude results of dual-band embedded elliptical patch reflecting element with different element spacing P are shown in Fig. 6. The cross-pol amplitude in C-band increase but that in X-band decrease with P increases. The relative good reflected amplitude can be obtained with the element spacing

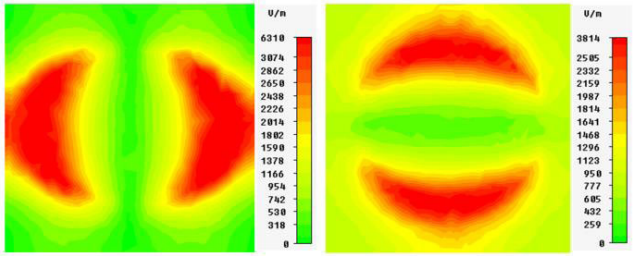

(a) (b)

FIGURE 5. Electric field distribution diagrams of the surface of the X-band embedded single elliptical patch reflecting element under (a) horizontally polarized plane wave, and (b) vertically polarized plane wave incidence.

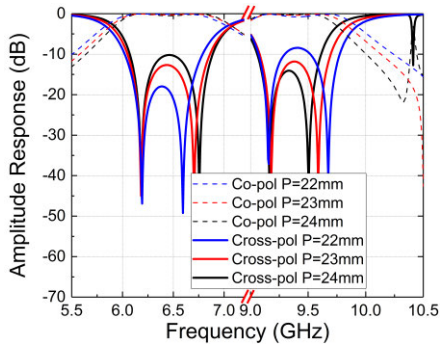

FIGURE 6. Reflected amplitude of the proposed dual-band embedded elliptical patch reflecting element for different element spacing values.

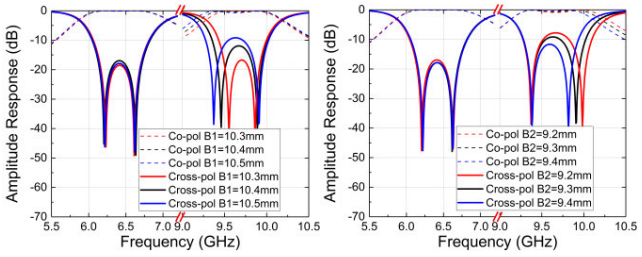

(a) (b)

FIGURE 7. Reflected amplitude of the proposed dual-band embedded elliptical patch reflecting element for (a) different major axis, and (b) different minor axis of the X-band element.

P is chosen to be 23 mm, which is equal to $0.475\lambda_{\text{lower}}$ at 6.2 GHz and $0.713\lambda_{\text{higher}}$ at 9.3 GHz.

For the proposed dual-band reflecting element, the amplitude responses are analyzed and optimized with different dimensions of the patches under the circularly polarized plane wave excitation. The results for the different dimensions of X-band elliptical patch are shown in Fig. 7. When the length of the major axis B_1 increases, keeping B_2 equal to 9.3 mm, the frequency with low co-pol reflection loss expands toward low frequency in the X-band. And when the length of the minor axis B_2 increases with B_1 is 10.5 mm, the frequency with low co-pol reflection loss expands toward high frequency in the X-band. The cross-pol reflected amplitude of the center frequency increase with B_1 increases and B_2 decreases. The similar regular can also be obtained for the C-band elliptical patch. The reflected amplitude of the element can be optimized by adjusting the length of the major and minor axis of the elliptical patches. In Fig. 7, the relative good reflected amplitude can be obtained with $B_1 = 10.4$ mm, $B_2 = 9.3$ mm. In addition, from Fig. 7, when the size of the X-band patch is changed, the reflected amplitude of the C-band patch change little, which can preliminary illustrate the low coupling effect between the two band patches.

TABLE 1. Optimized parameters.

parameter	A_1	A_2	B_1	B_2	H_1	H_2	p
value (mm)	17	14.45	10.4	9.3	0.787	1.575	23

The designed dual-band reflecting element is simulated and optimized by the frequency domain solver. The simulated model is shown in Fig. 1 (c). The boundary condition is set as unit cell to emulate the element in the periodic environment. The left-handed circularly polarized plane wave is adopted and excited by the Floquet port. The reflected phase in C- and X-band is responded to the rotation angle φ_l and φ_u, respectively. The optimized parameters of the dual-band reflecting element are summarized in Table 1.

B. ELEMENT PERFORMANCE

The reflected amplitude and phase response of the dual-band elliptical patch reflecting element is analyzed with the rotation angle φ_l and φ_u changed in steps of 10° under left-handed circularly polarized plane wave incidence. The two-dimensional co-pol reflected amplitude and phase response curves are shown in Fig. 8, where φ_l is shown at 6.2 GHz and φ_u is shown 9.3 GHz, under normal and 20° oblique incidence. At 6.2 GHz, the co-polar reflected phase response is only controlled by the rotation angle φ_l under normal and 20° oblique incidence, which is seen by the almost completely horizontal contour curves as shown in Fig. 8 (a)-(b). For a fixed rotation angle φ_u, the linear 360° phase variation is realized with φ_l varying from 0 to 180°. The co-polar reflected amplitude keeps more than −0.14 dB and is very stable as shown in Fig. 8 (c)-(d). And the results under normal incidence are consistent with those under 20° oblique incidence.

At 9.3 GHz, the co-polar reflected phase responses are almost completely vertical contour curves as shown in Fig. 8 (e)-(f), which indicate that the reflected phase only has to do with the rotation angle φ_u. For a fixed rotation angle φ_l, the linear 360° phase variation is also achieved with φ_u varying from 0 to 180°. As shown in Fig. 8 (g)-(h), the co-polar reflected amplitude under normal and 20° oblique incidence keeps more than −0.78 dB. The uniformity is also good except at some rotation angle φ_u under 20° oblique incidence. The reflected amplitude response in the both bands is little impacted by rotation angle φ_l and φ_u. Under different incident angles, the dual-band reflecting element obtains good reflected amplitude and phase response.

The coupling effect is important to the dual-band antenna. In general, the coupling effect refers to the maximum phase

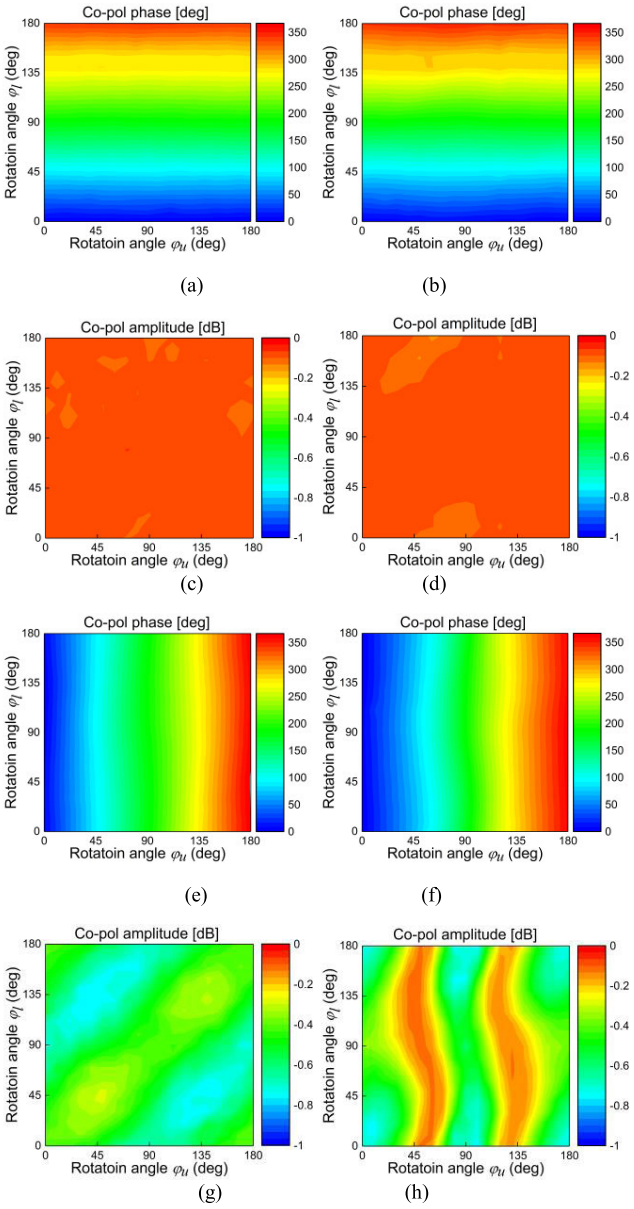

FIGURE 8. Two-dimensional co-pol reflected amplitude and phase of the proposed dual-band embedded elliptical patch reflecting element. At 6.2 GHz, amplitude response (a) under normal incidence and (b) under 20° oblique incidence, phase response (c) under normal incidence and (d) under 20° oblique incidence. At 9.3 GHz, amplitude response (e) under normal incidence and (f) under 20° oblique incidence, phase response (g) under normal incidence and (h) under 20° oblique incidence.

change for one frequency band element caused by adjusting another frequency band element. According to Fig. 8, the maximum phase change for the C-band element is 6° with the rotation of the X-band element, and for the X-band element is 8°. To illustrate the advantage of the proposed dual-band reflecting element, the representative single-layer dual-band reflecting elements [9], [12], [13] are analyzed with the same simulated method for comparison. To illustrate the power capacity level of the designed element, the models are scaled to work in the same frequencies and the scaled models are also simulated and compared. The obtained

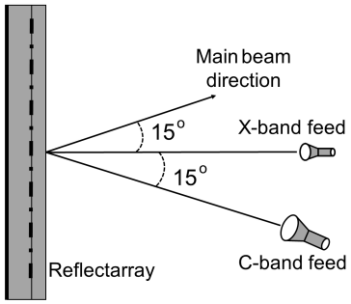

FIGURE 9. Schematic view of the dual-band reflectarray antenna.

mutual coupling effect and electric field results are shown in Table 2. The proposed element shows better mutual coupling effect and power capacity performance with respect to the other three designs.

III. REFLECTARRAY ANTENNA EXPERIMENTS AND SIMULATIONS

To verify the performance of the proposed dual-band reflecting element, a reflectarray antenna prototype with the aperture size of 345 mm × 345 mm is designed. The schematic view of the dual-band reflectarray antenna is shown in Fig. 9. To mitigate the blocking effect of the feeds, the C-band left-handed circularly polarized feed horn is titled 15° away from the boreside direction of the reflectarray for the relatively larger aperture, while the X-band left-handed circularly polarized feed horn is center-fed. The main beams at both bands are set to focus at the specular 15° direction to further minimize the feed blockage. In order to balance the illumination and spillover efficiencies, the position of the two feeds should be optimized with the edge taper of about −10 dB. The X-band feed horn is located at the height of 300 mm and the C-band feed horn is located at the height of 255 mm above the reflectarray aperture. The required phase shift over the reflectarray aperture can be calculated by the ray-tracing method [7],

$$\varphi_{mn} = k \cdot (r_{f\,\mathrm{mn}} - \hat{u}_0 \cdot \vec{r}_{mn}) + \varphi_{ref} \tag{1}$$

where k is the free space wavenumber, r_{fmn} is path distance between the feed and the mn^{th} element, $\hat{u}_0$ is the unit vector of required main beam direction, $\vec{r}_{mn}$ is the position vector of mn^{th} element, and φ_{ref} is the reference phase. The obtained progressive phase distributions at 6.2 GHz and 9.3 GHz on the reflectarray aperture are shown in Fig. 10 (a)-(b). Correspondingly, the elements are rotated to realize the pencil beam in the two bands according to Fig. 8 and the fabricated reflectarray aperture is shown in Fig. 10 (c). Full-wave simulations are carried out. The reflectarray antenna prototype is measured in an anechoic chamber. The prototypes of the fabricated dual-band reflectarray antenna in measurement setup are shown in Fig. 11. The epoxy resin skeleton forms the support structure to reduce the impact on the radiation pattern.

TABLE 2. Comparison of representative reports on single-layer dual-band reflecting elements.

Ref.	Mutual Coupling (deg)		Maximum E-field on Surface (V/m)		Maximum E-field on Surface [scaled model] (V/m)	
[9]	19.95 GHz <20	29.75 GHz >100	19.95 GHz 581,300	29.75 GHz 814,582	6.2 GHz 209,749	9.3 GHz 294,464
[12]	11.7 GHz >80	13.7 GHz >80	11.7 GHz 46,832	13.7 GHz 58,235	6.2 GHz 15,319	9.3 GHz 26,849
[13]	35 GHz >80	94 GHz <20	35 GHz 690,500	94 GHz 3459,000	6.2 GHz 110,613	9.3 GHz 215,779
This work	**6.2 GHz <6**	**9.3 GHz <8**	**6.2 GHz 4,203**	**9.3 GHz 7,928**	**6.2 GHz 4,203**	**9.3 GHz 7,928**

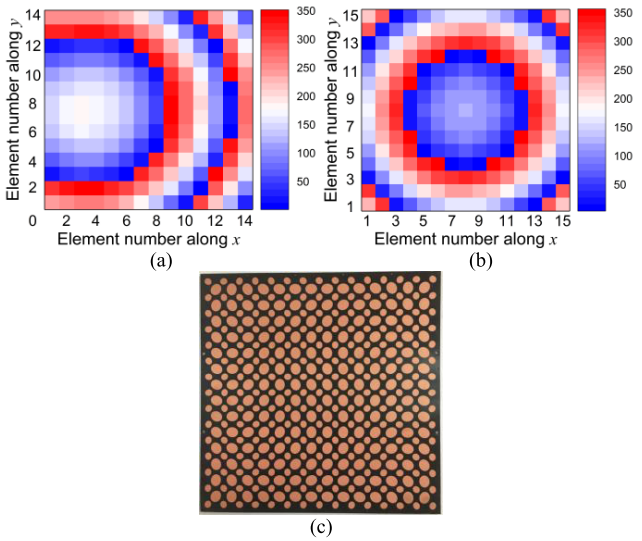

FIGURE 10. Progressive phase distributions on the reflectarray aperture (a) at 6.2 GHz, and (b) at 9.3 GHz. (c) Corresponding reflectarray aperture configuration.

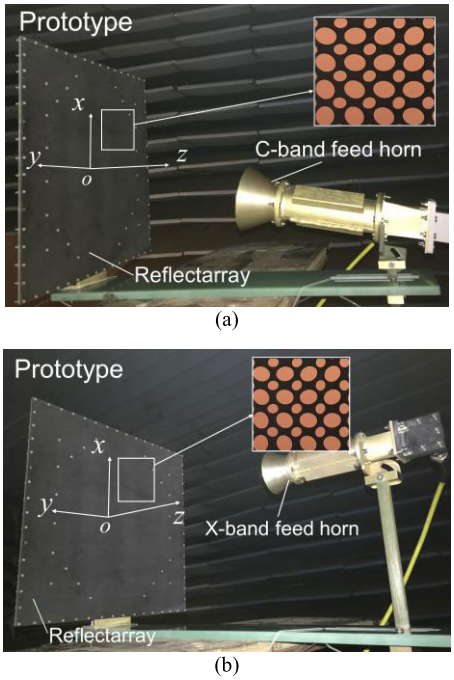

FIGURE 11. Prototypes of the dual-band reflectarray antenna in measurement setup at (a) C-band, and (b) X-band.

A. RADIATION PERFORMANCE ANALYSIS

The measured and simulated radiation patterns at the center frequency of 6.2 GHz and 9.3 GHz are shown in Fig. 12. The measured main lobes are well consistent with the simulated results with a little discrepancy for the first sidelobe and beyond. The reason for the discrepancy is that there are some differences between simulation and experiment in detail, such as the errors of assembling, fabrication, and measurement. The discrepancy is generally acceptable with the errors. At 6.2 GHz, the sidelobe level is −18 dB, and the −3 dB beamwidth is 8.7°. At 9.3 GHz, the sidelobe level is −15.3 dB, and the −3 dB beamwidth is 5.8°. Both at 6.2 GHz and 9.3 GHz, the pencil beams at the specified direction are realized, which verify the dual-band performance of the reflectarray antenna.

The measured and simulated gain and axial ratio results at different frequencies are shown in Fig. 13. At 6.2 GHz, the simulated gain is 24.9 dBi, the measured axial ratio is 0.7 dB, the measured gain is 24.6 dBi and the corresponding aperture efficiency is 51.8%. At 9.3 GHz, the simulated gain is 27.7 dBi, the measured axial ratio is 2.5 dB, the measured gain is 27.8 dBi and the aperture efficiency is 42%. In C-band, the measured 3 dB-gain bandwidth is in the frequency band of 5.7-6.7 GHz, and the measured axial ratio is lower than 3.8 dB in the above-mentioned frequency band. In X-band, the measured 3 dB-gain bandwidth is in the frequency band of 8.65-9.55 GHz, and the measured axial ratio is lower than 2.8 dB. The measured results are in good agreement with the simulated results, which verify the radiation performance of the antenna.

B. COUPLING EFFECT ANALYSIS

To further verify the low coupling effect of the antenna, the single-frequency reflectarray antennas that only contain the C-band or X-band patches are simulated and designed with the same aperture size for comparison. The simulated radiation patterns are shown in Fig.14. At 6.2 GHz, the gain of the C-band only reflectarray antenna is 24.5 dBi, which is reduced by 0.4 dBi compared to the dual-band reflectarray antenna. At 9.3 GHz, the gain of the X-band only reflectarray antenna is 28.3 dBi, which is increased by 0.5 dBi compared to the dual-band reflectarray antenna. The radiation patterns

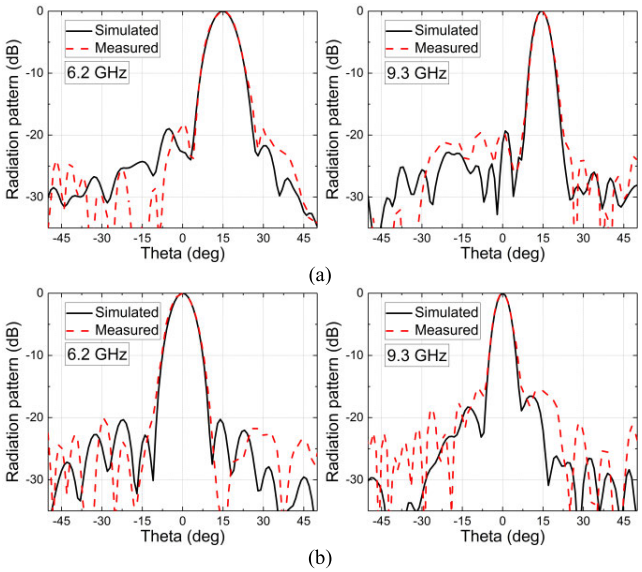

FIGURE 12. Measured and simulated radiation patterns in (a) *xoz* plane, and (b) orthogonal plane at 6.2 GHz and 9.3 GHz.

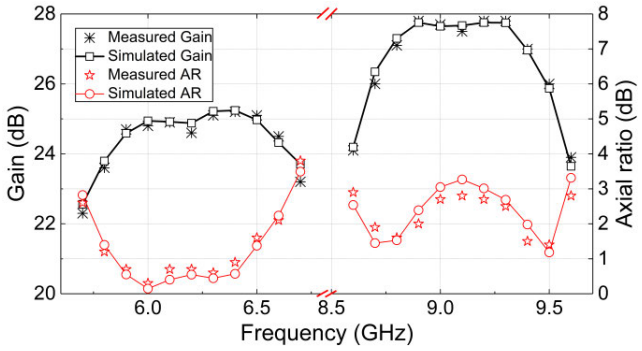

FIGURE 13. Measured and simulated gains and axial ratios at various frequencies.

of the single band reflectarray antennas are consistent well with those of the dual-band reflectarray antennas, and the gain change is less than 0.5 dBi, which can verify the low mutual coupling performance of the dual-band reflectarray antenna.

C. POWER HANDLING CAPACITY ANALYSIS

The formula of power handling capacity calculation is as follow [18]:

$$P_{\max} = P_{\text{in}} \cdot (E_b/E_{\max})^2 \tag{2}$$

which $P_{\max}$ is power handling capacity, P_{in} is input power, E_b is breakdown threshold value and $E_{\max}$ is maximum field strength.

At the two operating frequencies, the obtained electric field distribution diagrams of the embedded patches and the surface of the reflectarray are shown in Fig. 15. The input power is 0.5 W. At 6.2 GHz, the maximum electric field of the embedded patch is 2153 V/m, and the maximum electric field on the surface of the reflectarray is 665 V/m, which is about a quarter of that in the patch and significantly improves the power capacity of the antenna. The

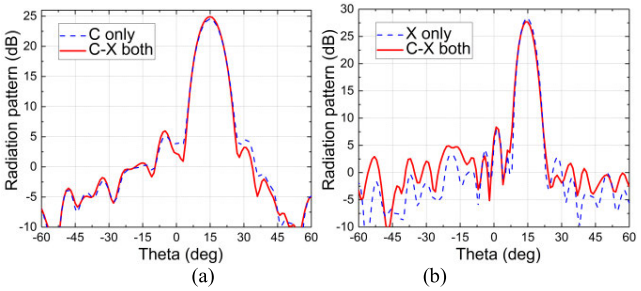

FIGURE 14. Simulated radiation patterns in *xoz* plane at (a) 6.2 GHz, and (b) 9.3 GHz.

TABLE 3. Comparison of the previous reports on high power reflectarray antennas.

Ref.	[7]	[19]	[20]	**This work**
Aperture Dimension	5.8λ	8.4λ	8.2λ	**6.7λ/10.7λ**
Frequency (GHz)	9.3	10	10	**6.2/9.3**
Measured Gain (dB)	23.4	21.66	20.2	**24.6/27.8**
Side-lobe Level(dB)	-15.8	-10	-12	**-18/-15.3**
Aperture Efficiency	50.6%	15.5%	11.8%	**51.8%/42%**
Power Capacity under Air Condition	0.5MW	1.02MW	2.7MW	**10.2 MW /3.9 MW**

calculated power handling capacity of the embedded patches is $(4 \times 10^7/2153)^2 \times 0.5$ W = 172.6 MW, which is based on the substrate breakdown threshold of 40 MV/m [18]. The calculated power handling capacity of the surface of the reflectarray is $(3 \times 10^6/665)^2 \times 0.5$ W = 10.2 MW, which is based on the breakdown threshold of air that is 3 MV/m. At 9.3 GHz, the maximum electric field of the embedded patch is 3295 V/m, and the maximum electric field on the surface of the reflectarray is 1071 V/m. The calculated power capacity of the embedded patches is $(4 \times 10^7/3295)^2 \times 0.5$ W = 73.7 MW. The calculated power handling capacity of the surface of the reflectarray is $(3 \times 10^6/1071)^2 \times 0.5$ W = 3.9 MW under air condition. For the two operating frequencies, the power capacities are limited by the surface of the reflectarray. To improve the power capacity, it is easy to mount a radome on the reflectarray to fill one atm of SF_6 gas with the breakdown threshold value of 11 MV/m. Under one atm of SF_6 gas, the calculated power handling capacity of the surface of the reflectarray is $(1.1 \times 10^7/665)^2 \times 0.5$ W = 136.8 MW for 6.2 GHz. As for 9.3 GHz, the calculated power handling capacity of the surface of the reflectarray is $(1.1 \times 10^7/1071)^2 \times 0.5$ W = 52.7 MW.

In general, the thermal issue is not the main issue to be considered in the high-power microwave field. The duty cycle of the high-power microwave pulsed is sufficient low and the average power is not high. So it should not cause a huge change in the temperature to affect the configuration of the antenna and thermal effects can be ignored.

D. COMPARISON WITH OTHER HIGH-POWER REFLECTARRAY ANTENNAS

The comparison on some previous reports of high-power reflectarray antennas is shown in Table 3. The proposed

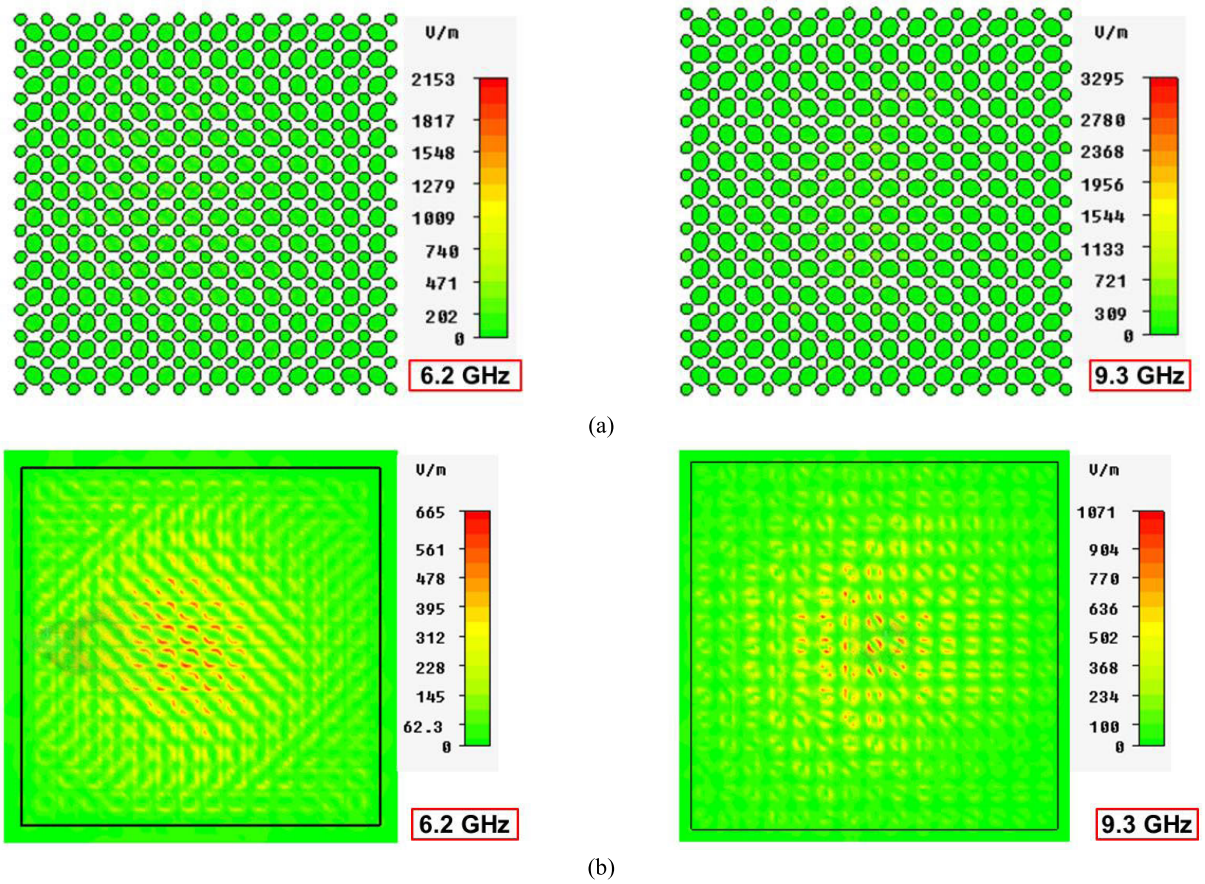

FIGURE 15. Electric field distribution diagrams of (a) the patches, and (b) the surface of the reflectarray at 6.2 GHz and 9.3 GHz.

reflectarray antenna shows higher power capacity than the other three designs [7], [19], [20]. And the proposed reflectarray antenna shows higher aperture efficiency and lower sidelobe level than the designs in [19] and [20]. Furthermore, the proposed design can work in two frequency bands with the frequency ratio of 1.5, but the other three designs can only work in one frequency band.

IV. CONCLUSION

This letter presents a patch reflectarray antenna to realize the dual-band feature of high-power antennas. Since the patches of the traditional reflecting element generally are exposed to the air and with the structure of splits or slots, their power capacity is limited. To solve this problem, the elliptical patch with no abrupt structure is proposed to be embedded into substrate. And two embedded elliptical patches with different sizes are proposed to be arranged in a square lattice grid to be the high-power dual-band reflecting element. The dual-band reflecting element has not only high-power capacity but also low mutual coupling. In addition, the angular rotation technique is demonstrated can be applied to the elliptical patch element to realize the linear 360° phase shift. To verify the performance of the proposed element, a reflectarray antenna prototype is designed, simulated, and measured in both C-band and X-band. The measured results are in good agreement with simulations, which can validate the proposed design and its practical realization of dual-band high-power microwave antenna applications.

REFERENCES

[1] D. Giri, *High-Power Electromagnetic Radiators: Nonlethal Weapons and Other Applications*. Cambridge, MA, USA: Harvard Univ. Press, 2004.
[2] C.-W. Yuan, S.-R. Peng, T. Shu, Z.-Q. Li, and H. Wang, "Designs and experiments of a novel radial line slot antenna for high-power microwave application," *IEEE Trans. Antennas Propag.*, vol. 61, no. 10, pp. 4940–4946, Oct. 2013.
[3] Y. Liang, J. Zhang, Q. Liu, and X. Li, "High-power radial-line helical subarray for high-frequency applications," *IEEE Trans. Antennas Propag.*, vol. 66, no. 8, pp. 4034–4041, Aug. 2018.
[4] Y. Liang, J. Zhang, Q. Liu, and X. Li, "High-power dual-branch helical antenna," *IEEE Antennas Wireless Propag. Lett.*, vol. 17, no. 3, pp. 472–475, Mar. 2018.
[5] X.-Q. Li, Q.-X. Liu, X.-J. Wu, L. Zhao, J.-Q. Zhang, and Z.-Q. Zhang, "A GW level high-power radial line helical array antenna," *IEEE Trans. Antennas Propag.*, vol. 56, no. 9, pp. 2943–2948, Sep. 2008.
[6] L. Guo, W. Huang, C. Chang, J. Li, Y. Liu, and R. Meng, "Studies of a leaky-wave phased array antenna for high-power microwave applications," *IEEE Trans. Plasma Sci.*, vol. 44, no. 10, pp. 2366–2375, Oct. 2016.
[7] G. Kong, X. Li, Q. Wang, and J. Zhang, "A wideband reconfigurable dual-branch helical reflectarray antenna for high-power microwave applications," *IEEE Trans. Antennas Propag.*, vol. 69, no. 2, pp. 825–833, Feb. 2021.
[8] M. R. Chaharmir and J. Shaker, "Design of a multilayer X-/Ka-band frequency-selective surface-backed reflectarray for satellite applications," *IEEE Trans. Antennas Propag.*, vol. 63, no. 4, pp. 1255–1262, Apr. 2015.
[9] T. Smith, U. Gothelf, O. S. Kim, and O. Breinbjerg, "Design, manufacturing, and testing of a 20/30-GHz dual-band circularly polarized reflectarray antenna," *IEEE Antennas Wireless Propag. Lett.*, vol. 12, pp. 1480–1483, 2013.

[10] Z. Hamzavi-Zarghani and Z. Atlasbaf, "A new broadband single-layer dual-band reflectarray antenna in X- and ku-bands," *IEEE Antennas Wireless Propag. Lett.*, vol. 14, pp. 602–605, 2015.
[11] R. S. Malfajani and Z. Atlasbaf, "Design and implementation of a dual-band single layer reflectarray in X and K bands," *IEEE Trans. Antennas Propag.*, vol. 62, no. 8, pp. 4425–4431, Aug. 2014.
[12] L. Guo, P.-K. Tan, and T.-H. Chio, "Single-layered broadband dual-band reflectarray with linear orthogonal polarizations," *IEEE Trans. Antennas Propag.*, vol. 64, no. 9, pp. 4064–4068, Sep. 2016.
[13] Q. Wang, Z. H. Shao, Z. X. Fang, S. Feng, Y. J. Cheng, and P. K. Li, "Low cost single layer dual band dual linear polarization reflectarray antenna," in *Proc. Asia–Pacific Microw. Conf.*, Nanjing, China, Dec. 2015, pp. 1–3.
[14] S. R. Lee, E. H. Lim, F. L. Lo, and W. H. Ng, "Circularly polarized elliptical microstrip patch reflectarray," *IEEE Trans. Antennas Propag.*, vol. 65, no. 8, pp. 4322–4327, Aug. 2017.
[15] C. A. Balanis, *Antenna Theory: Analysis and Design*. New York, NY, USA: Harper and Row, 1982, pp. 859–865.
[16] S. Peng, C. Yuan, T. Shu, and X. Zhao, "Linearly polarised radial line slot antenna for high-power microwave application," *IET Microw., Antennas Propag.*, vol. 11, no. 5, pp. 680–684, Apr. 2017.
[17] P. Nayeri, F. Yang, and A. Z. Elsherbeni, *Reflectarray Antennas: Theory, Designs, and Applications*. Hoboken, NJ, USA: Wiley, 2018.
[18] X. Li, Z. Zhou, Q. Wang, and J. Zhang, "A polarization conversion radome for high-power microwave applications," *IEEE Antennas Wireless Propag. Lett.*, vol. 18, no. 6, pp. 1096–1099, Jun. 2019.
[19] S. A. Tazehabadi and S. Jam, "X-band reflectarray antenna with arbitrarily (elliptical) polarization for high-power microwave applications," *Eng. Sci. Technol., Int. J.*, vol. 23, no. 3, pp. 585–594, Jun. 2020.
[20] S. A. Tazehabadi and S. Jam, "A high-power microwave reflectarray antenna based on perforated dielectric substrate," *Adv. Electromagn.*, vol. 8, no. 1, pp. 16–22, Mar. 2019.

GEXING KONG was born in Henan, China, in September 1991. He received the B.E. degree in applied physics from Shangqiu Normal University, Henan, in 2015. He is currently pursuing the Ph.D. degree in radio physics with Southwest Jiaotong University, Chengdu.

His current research interests include antennas, microwave windows, and microwave mode conversion.

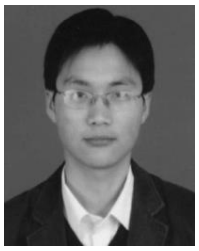

XIANGQIANG LI (Member, IEEE) was born in Shandong, China, in October 1982. He received the B.E. and Ph.D. degrees from the School of Physical Science and Technology, Southwest Jiaotong University, Chengdu, China, in 2003 and 2008, respectively.

He is currently a Professor with the School of Physical Science and Technology, Southwest Jiaotong University. His current research interests include antennas and microwave components.

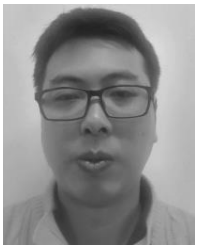

QINGFENG WANG was born in Fujian, China, in 1979. He received the M.Sc. and Ph.D. degrees from Southwest Jiaotong University, Chendu, China, in 2006 and 2011, respectively.

He is currently a Professor with the School of Physical Science and Technology, Southwest Jiaotong University. His current research interests include high-voltage technology and electromagnetic compatibility.

JIANQIONG ZHANG was born in Sichuan, China, in April 1983. He received the B.S. and the Ph.D. degrees from Southwest Jiaotong University, Chengdu, China, in 2005 and 2011, respectively.

He is currently a Professor with the School of Physical Science and Technology, Southwest Jiaotong University. His current research interests include antennas and electromagnetic compatibility.